Journal of Ginseng Research 48 (2024) 190–201

Contents lists available at ScienceDirect

Journal of Ginseng Research

journal homepage: www.sciencedirect.com/journal/journal-of-ginseng-research

Research Article

# Reciprocal regulation of SIRT1 and AMPK by Ginsenoside compound K impedes the conversion from plasma cells to mitigate for podocyte injury in MRL/*lpr* mice in a B cell-specific manner

Ziyu Song [a,1], Meng Jin [a,1], Shenglong Wang [a,1], Yanzuo Wu [a,1], Qi Huang [b], Wangda Xu [a], Yongsheng Fan [c,*], Fengyuan Tian [a,d,**]

[a] First School of Clinical Medicine, Zhejiang Chinese Medical University, Hangzhou, China
[b] Department of Endocrinology, The First Affiliated Hospital of Zhejiang Chinese Medical University, Hangzhou, China
[c] College of Basic Medical Science, Institute of Basic Research in Clinical Medicine, Zhejiang Chinese Medical University, Hangzhou, China
[d] General Practice, The First Affiliated Hospital of Zhejiang Chinese Medical University, Hangzhou, China

ARTICLE INFO

*Keywords:*
Ginsenoside CK
Lupus nephritis
Podocyte
Plasma cell

ABSTRACT

*Background:* Deposition of immune complexes drives podocyte injury acting in the initial phase of lupus nephritis (LN), a process mediated by B cell involvement. Accordingly, targeting B cell subsets represents a potential therapeutic approach for LN. Ginsenoside compound K (CK), a bioavailable component of ginseng, possesses nephritis benefits in lupus-prone mice; however, the underlying mechanisms involving B cell subpopulations remain elusive.

*Methods:* Female MRL/*lpr* mice were administered CK (40 mg/kg) intragastrically for 10 weeks, followed by measurements of anti-dsDNA antibodies, inflammatory chemokines, and metabolite profiles on renal samples. Podocyte function and ultrastructure were detected. Publicly available single-cell RNA sequencing data and flow cytometry analysis were employed to investigate B cell subpopulations. Metabolomics analysis was adopted. SIRT1 and AMPK expression were analyzed by immunoblotting and immunofluorescence assays.

*Results:* CK reduced proteinuria and protected podocyte ultrastructure in MRL/*lpr* mice by suppressing circulating anti-dsDNA antibodies and mitigating systemic inflammation. It activated B cell-specific SIRT1 and AMPK with Rhamnose accumulation, hindering the conversion of renal B cells into plasma cells. This cascade facilitated the resolution of local renal inflammation. CK facilitated the clearance of deposited immune complexes, thus reinstating podocyte morphology and mobility by normalizing the expression of nephrin and SYNPO.

*Conclusions:* Our study reveals the synergistic interplay between SIRT1 and AMPK, orchestrating the restoration of renal B cell subsets. This process effectively mitigates immune complex deposition and preserves podocyte function. Accordingly, CK emerges as a promising therapeutic agent, potentially alleviating the hyperactivity of renal B cell subsets during LN.

## 1. Introduction

The pathogenesis of lupus nephritis (LN) hinges upon the pivotal role of autoantibodies [1]. Gaining insights into the changes within the proliferation and differentiation of B cell subpopulations could unravel the intricate landscape of this specific lymphocyte subset in the context of LN [2]. An increasing body of evidence suggests the potential of B cell-targeting therapies to mitigate renal damage in LN [3–5]. Of notable importance are plasma cells, responsible for sustaining elevated levels of pathogenic autoantibodies that drive inflammation, independent of antigen stimulation and T-cell assistance [6,7]. Their recruitment from the spleen inflicts sustained harm on the renal microenvironment, directed by a circulating chemokine gradient [8]. Mechanistically, the hyperactive involvement of B cell subsets undergoes a branching

* Corresponding author. College of Basic Medical Science, Institute of Basic Research in Clinical Medicine, Zhejiang Chinese Medical University, Hangzhou, PR China.
** Corresponding author. First School of Clinical Medicine, Zhejiang Chinese Medical University, Hangzhou, PR China.
*E-mail addresses:* fyszjticm@163.com (Y. Fan), hztfy526@126.com (F. Tian).
[1] These authors have contributed equally to this work.

https://doi.org/10.1016/j.jgr.2023.11.006
Received 28 June 2023; Received in revised form 27 November 2023; Accepted 28 November 2023
Available online 3 December 2023

cascade, giving rise to germinal center B cells, plasma cells, and memory B cells. This cascade facilitates the renal accumulation of immune complexes, a crucial prerequisite for in situ inflammation [2]. Consequently, this progression culminates in the effacement of foot processes, marked by cytoskeletal disruption, leading to podocyte apoptosis and detachment [9]. This initial step triggers irreversible renal damage [10]. Recognizing the pivotal role of plasma cells, strategies targeting the inhibition of plasma cell conversion have emerged as promising avenues to address proteinuria and podocyte injury in LN [3].

Sirtuin 1 (SIRT1), a multifunctional histone deacetylase within the sirtuin family, orchestrates diverse biological processes, including immune responses, oxidative stress, and energetic homeostasis [11,12]. It has been established that specific depletion of SIRT1 exacerbates podocyte injury by impairing autophagy [13]. Conversely, its overexpression effectively interrupts lipid accumulation, thereby preserving podocyte structure and function [14]. SIRT1 expression fluctuates during the proliferation and differentiation of B cell subpopulations. It rises in resting B cells but is silenced upon the commitment to the immunoglobulin class switch [15]. Therefore, investigating SIRT1's involvement in B cell subsets within the downstream network warrants exploration in detail. Adenosine monophosphate-activated protein kinase (AMPK), a key player in energy sensing, exhibits crosstalk with SIRT1 [16]. Recent studies have highlighted AMPK activation as a deterrent against B cell differentiation into autoreactive plasma cells [17]. Thus, unraveling the functional interplay between SIRT1 and AMPK during the dynamic conversion of renal B cell compensation across relevant subtypes might be an appealing therapeutic approach for LN remission.

Ginsenoside Compound K (CK, *20-O-b-D-glucopyranosyl20(S)-protopanaxadiol*), an absorbable bioavailable component of ginseng, derives from ginsenosides Rb1, Rb2, Rc, and Rd through gut microbiota-driven biotransformation [18]. Numerous reports indicated that CK confers reliable metabolic benefits with increased phosphorylation of AMPK, leaning on its potent anti-inflammatory properties [19–22]. Prior studies revealed that CK suppresses NLRP3 inflammasome activation via autophagy modulation coupled with Th cell modulation in NZB/WF1 mice [23]. However, comprehensive exploration and validation of this mechanism, especially in the context of B cell subset differentiation, with emphasis on the SIRT1/AMPK axis, remain essential. The MRL/*lpr* mouse strain is a validated model of lupus nephritis, mirroring humanized lupus with progressive glomerulonephritis [24]. Based on an open-source single-cell RNA sequencing dataset [2], our study sought to elucidate CK's anti-inflammatory effects on renal remission and its potential to delay B cell activation and conversion into plasma cells underlying the network of SIRT1 and AMPK.

## 2. Materials and methods

### 2.1. Animals and treatments

Female MRL/*MpJ*-Fas*lpr*/J (MRL/*lpr*) and MRL/*MpJ* mice (4 weeks old) were procured from Shanghai SLAC Laboratory Animal Co., Ltd (Shanghai, China). All mice were randomly assigned to three groups ($n$ = 6 per group). CK (molecular weight 622.87 Da, purity ≥99.0 %) was purchased from Shanghai Winherb Medical Science Co., Ltd. (Shanghai, China). In the CK group, mice received intragastric administration of CK (40 mg/kg) dissolved in 0.5 % CMC-Na once daily, following the previously outlined dosage protocol [19,25]. The remaining mice were given an equivalent volume of CMC-Na. At the end of a 10-week intervention period, all mice were euthanized using pentobarbital overdose following the monitoring and approval of animal welfare by the Institutional Animal Care and Use Committee of Zhejiang Chinese Medical University.

### 2.2. Enzyme-linked immunosorbent assay (ELISA)

Concentrations of TNF-α, IL-6, IL-10, CXCL12, CXCL13, CCL19, and anti-dsDNA were assessed using corresponding ELISA kits (Cusabio, Wuhan, China). Standard ELISA protocols were followed to analyze serum samples, following the kit instructions.

### 2.3. Flow cytometry

Single-cell suspensions of splenic or renal cells were isolated from MRL/*MpJ* or MRL/*lpr* mice. The splenic and renal samples were triturated sequentially, passed through a 70-mesh sieve, and then treated with red blood cell (RBC) lysis buffer (BioLegend, CA, USA). B cells were depleted through magnetic bead separation using the EasySep CD19-positive selection II kit (Stemcell, Canada). The renal samples were incubated with 0.5 mg/mL Collagenase IV and 0.1 mg/mL DNase I in RPMI-1640 medium for 30 min at 37 °C with agitation. Subsequently, cells from the spleen and kidney were filtered, re-suspended in RPMI-1640 medium with 10 % FBS, and subjected to flow cytometry on the CytoFlex S (Beckman Coulter, Canada), following previously described protocols [26]. The classification of each subset was consistent with established literature-based markers [27,28].

### 2.4. RT-PCR analysis

Total RNA was extracted from renal and splenic samples using the Qiagen RNA extraction kit (Hilden, Germany). Reverse transcription into cDNA was accomplished using the SuperScript III kit (ThermoFisherScientific, CA, USA). Real-time PCR analysis, performed in sextuplicate, utilized the Roche LightCycler 96 SW1.1 instrument (Basel, Switzerland). Expression levels of target genes were normalized to *GAPDH* as an endogenous control. Mouse primer sequences for amplification were provided in Supplementary Table 1.

### 2.5. Biochemical analysis

Creatinine colorimetric assay kits (Nanjing Jiancheng, China) were used to quantify blood urea nitrogen (BUN) and creatinine (Cre) concentrations in serum following the manufacturer's instructions. The Bradford method (Nanjing Jiancheng) was used to determine urine protein and albumin levels.

### 2.6. Histopathological analysis

Kidneys were sectioned, fixed in a 4 % paraformaldehyde buffer solution, and embedded using established protocols. The tissue sections underwent various staining procedures, including hematoxylin and eosin (H&E), periodic acid-Schiff (PAS), and Masson staining. Renal lesion quantification was performed in a blinded manner, as previously described [29].

### 2.7. Cell culture

The conditionally immortalized mouse podocyte clone 5 (MPC-5) and the human Burkitt's Lymphoma cell line (Namalwa) were provided by the Shanghai Cell Bank of the Chinese Academy of Sciences (Shanghai, China). These cell lines were cultured in RPMI-1640 or DMEM medium supplemented with 10% fetal bovine serum (HyClone, UT, USA) and IFN-γ (10 IU/mL) within a humidified chamber maintained at 37 °C and 5% $CO_2$.

Briefly, both cell lines were exposed to various stimuli, including media alone, vehicle treatment, R848 (20 μM, MedchemExpress) alone, or a combination of CK (2 μM) and R848 (20 μM). Additionally, Namalwa cells underwent further stimulation using conventional stimulatory conditions [30].

### 2.8. Immunofluorescence staining

Frozen renal specimens underwent an initial blocking process.

Subsequently, sections were subjected to overnight incubation with primary antibodies, including IgG-FITC (Abcam, MA, USA), C3 (MP Biomedicals, CA, USA), TGF-β1 (CellSignalingTechnology, MA, USA), Smad3 (CellSignalingTechnology), nephrin (Invitrogen, CA, USA), SYNPO (Invitrogen), CD19 (CellSignalingTechnology), CD138 (CellSignalingTechnology), SIRT1 (CellSignalingTechnology), and AMPK (CellSignalingTechnology). After primary antibody incubation, the sections were treated with secondary antibodies, Alexa Fluor anti-rabbit 488 or Alexa Fluor anti-mouse 594 (Invitrogen), for 1 h. Nuclear staining was achieved using DAPI (Sigma-Aldrich, MO, USA). Assessment of MPC-5 cell apoptosis was conducted using the Click-It TUNEL kit (Invitrogen), following instructions. Finally, the specimens were visualized using an LSM700 Carl Zeiss confocal microscope (Jena, Germany).

### 2.9. Transmission electron microscopy (TEM)

Fresh renal cortex samples were dissected into small fragments measuring approximately 1 $mm^3$ for examination of ultrastructural alterations. These tissue fragments were fixed in a 2.5 % PBS-buffered glutaraldehyde solution. The samples were subsequently treated with 1 % osmium tetraoxide at 4 °C for 1 h. Subsequently, the tissues were dehydrated and sliced into ultrathin sections measuring 70 nm in thickness. The ultrastructural features were visualized at high resolution using a JEOL JEM-2100 transmission electron microscope (Tokyo, Japan).

### 2.10. Immunoblotting analysis

Renal samples and Namalwa cells were homogenized and lysed in RIPA buffer. Denatured proteins from the lysates were separated on SDS-PAGE gels and then transferred onto PVDF membranes. After blocking, the membranes were incubated overnight at 4 °C with primary antibodies: nephrin (Invitrogen), SYNPO (Invitrogen), SIRT1 (CellSignalingTechnology), AMPK (CellSignalingTechnology), *p*AMPK (CellSignalingTechnology), CPT1A (CellSignalingTechnology), and GAPDH (ThermoFisherScientific, MA, USA). Following primary antibody incubation, secondary antibodies were applied.

### 2.11. Wound-healing assay

MPC-5 cells were cultured overnight in a 6-well plate coated with type I collagen. A straight scratch was introduced into the cell monolayers using a 200 μl pipette tip. The cells were then incubated for 12 h to observe cell migration.

### 2.12. Human single-cell data analysis

Raw and normalized gene count matrices from both normal and lupus nephritis human kidney samples were extracted from a prior study [2]. These matrices were then integrated with the SCANPY ingest protocol, as previously described. After filtration, cell type annotations aligned with earlier datasets, including Villani et al. and FANTOM5, following established literature procedures [2]. Subsequently, UMAP dimensionality reduction was performed to analyze renal B cell subsets followed by gene set enrichment analysis utilizing the AUCell tool. Single-cell cluster gene enrichment analysis was performed with SCDE [31].

### 2.13. Renal metabolomics

Untargeted metabolomics analysis was conducted as previously described [32]. Briefly, thawed renal samples (200 μL) were mixed with a prechilled mixture [methanol: ethanediol (v/v, 5:5)] in the amount of 600 μL. After vigorous vortexing, the resultant precipitate was collected, vacuum-dried, and then reconstituted using a mixed solution [methanol: acetonitrile: ultrapure water, (v/v/v, 4:1:5)]. Further vortexing and centrifugation were performed, and an aliquot of 10 μL of the supernatant was collected for ultra-performance liquid chromatography-quadrupole/time of flight mass spectrometry (UPLC-Q/TOF-MS) analysis.

### 2.14. Molecular docking

To assess the binding affinity between CK and the target receptors (i.e., SIRT1 and AMPK), molecular docking analysis was performed using Autodock 1.5.7 software. Crystal structures of SIRT1 and AMPK were obtained from the protein database in RCSB PDB. The conformation exhibiting the lowest binding energy was visualized using PyMOL software.

### 2.15. Statistics

Experimental data were depicted as the mean ± standard error of the mean (SEM). Statistical analysis was performed using GraphPad Prism version 8.0 software (CA, USA), employing one-way analysis of variance (ANOVA) to identify group variations. Post hoc analysis was conducted using Turkey's method to assess the significance of differences between groups. Statistical significance was defined by *p*-values below 0.05 ($^*p < 0.05$; $^{**}p < 0.01$).

## 3. Results

### 3.1. CK alleviated lupus manifestations

To investigate the therapeutic effects of CK (Fig. 1A) on LN, an experimental model was implemented using lupus-susceptible female MRL/*lpr* mice, while MRL/*MpJ* mice were employed as the control group. CK was administered intragastrically to MRL/*lpr* mice from 9 to 18 weeks (Fig. 1B). MRL/*lpr* mice typically exhibited features of human SLE around 12 weeks [33]. Initially, the survival of the mice was monitored during the intervention period (Fig. 1C). Additionally, MRL/*lpr* mice displayed spontaneous splenomegaly and enhanced levels of anti-dsDNA antibodies, which were mitigated by CK treatment (Fig. 1D and E).

As expected, CK treatment substantially reduced elevated TNF-α and IL-6 levels while ameliorating suppressed IL-10 levels (Fig. 1F). Moreover, in MRL/*lpr* mice, there was an overall increase in B cell-related chemotactic chemokines (i.e., CXCL12, CXCL13, and CCL19) contributing to excessive B cell mobilization, while CK administration countered this accumulation to a certain extent (Fig. 1G).

### 3.2. CK re-established splenic B cell equilibrium

To delve into the B cell compensation driven by CK, we performed the flow cytometry analysis to examine the overall composition of relevant subsets within the mature B cell compartment in the spleen. Compared to controls, MRL/*lpr* mice exhibited reduced naive and mature B cells, as well as follicular (Fo) and marginal zone (Mz) B cells; memory B cell subpopulations (i.e., IgM, switched, and Late) also primarily evacuated from the B cell compartment, while the striking increase in plasma cells in response to lupus proneness (Fig. 2A). In contrast, CK treatment mitigated the loss of naive and switched memory B cells to some extent attenuating the increase in plasma cells (Fig. 2A).

Consistently, CK-treated mice displayed reduced expression of *PRDM1*, *IRF4*, *IKZF1*, and *TCF3*, but not *XBP1* and *EBF1*; while the expression of *BCL6*, *PAX5*, *IRF8*, and *BACH2* ascended (Fig. 2B). Furthermore, CK led to a general reduction in canonical inflammation and chemotaxis genes in splenic samples of MRL/*lpr* mice, aligning with improved lupus phenotypes (Fig. 2C). These findings suggest that CK contributes to autoinflammation resolution by diminishing the plasma cell population.

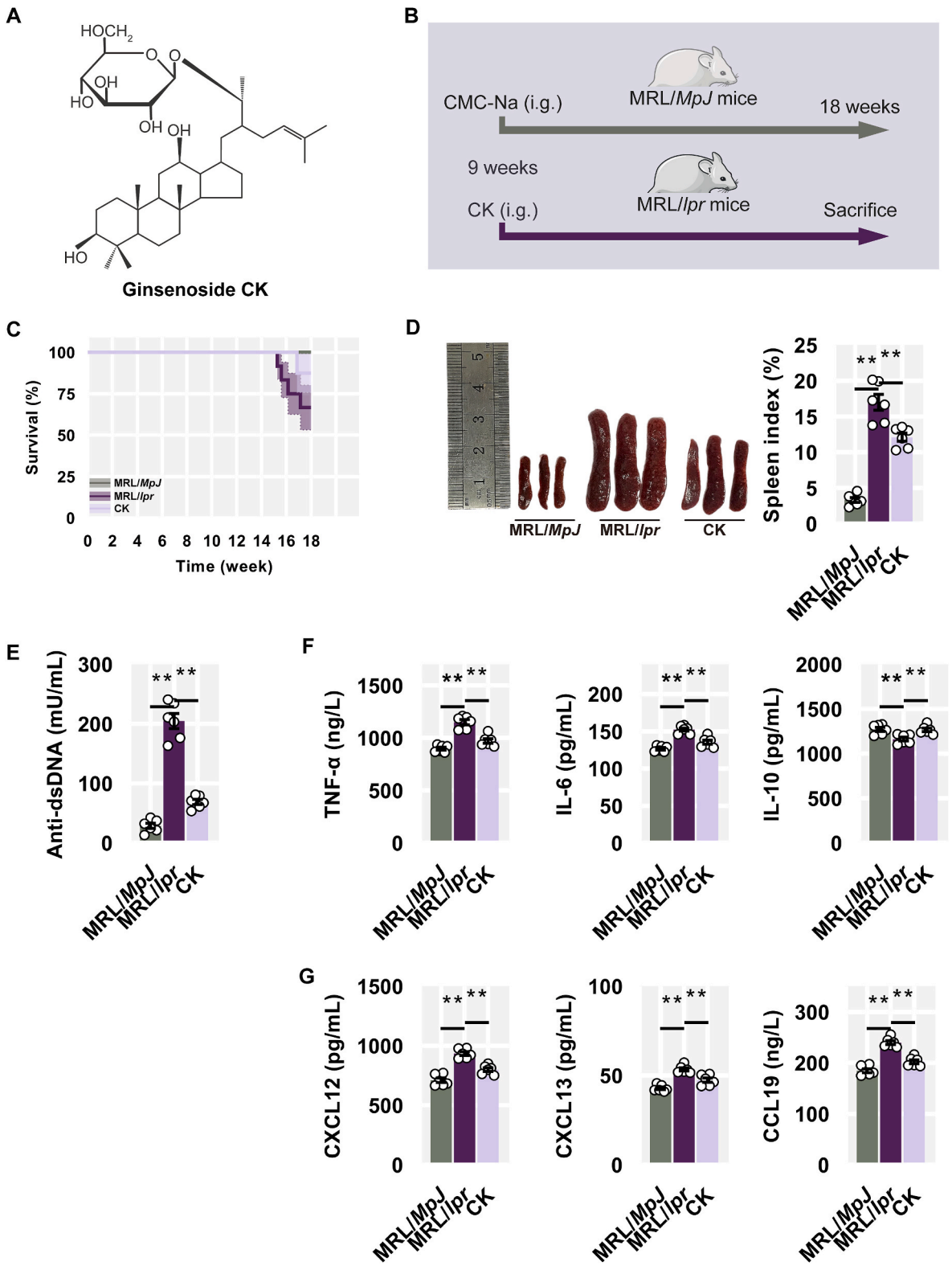


**Fig. 1.** CK alleviated lupus manifestations. (A) Chemical structure of CK. (B) Experimental scheme. (C) Overall survival curve. (D) Representative spleens and spleen indexes. (E) The levels of anti-dsDNA antibody. (F) The levels of TNF-α, IL-6, and IL-10. (G) The levels of CXCL12, CXCL13, and CCL19 in serum.

### *3.3. CK restores podocyte ultrastructure following renal damage*

We further evaluate and assess the renal function and pathological consequences by utilizing CK. MRL/*lpr* mice displayed severe proteinuria, with notable increases in total protein and albumin levels; notably, CK administration had a profound reduction in both (Fig. 3A). Additionally, CK-treated mice showed renoprotective effects with lower BUN and creatinine levels (Fig. 3A). Histological analysis of renal specimens from MRL/*lpr* mice revealed inflammatory cell infiltration, glomerular crescents, endocapillary proliferation, and significant collagen deposition; however, CK treatment prevented nephritic histopathology in MRL/*lpr* mice, thereby restoring renal architecture

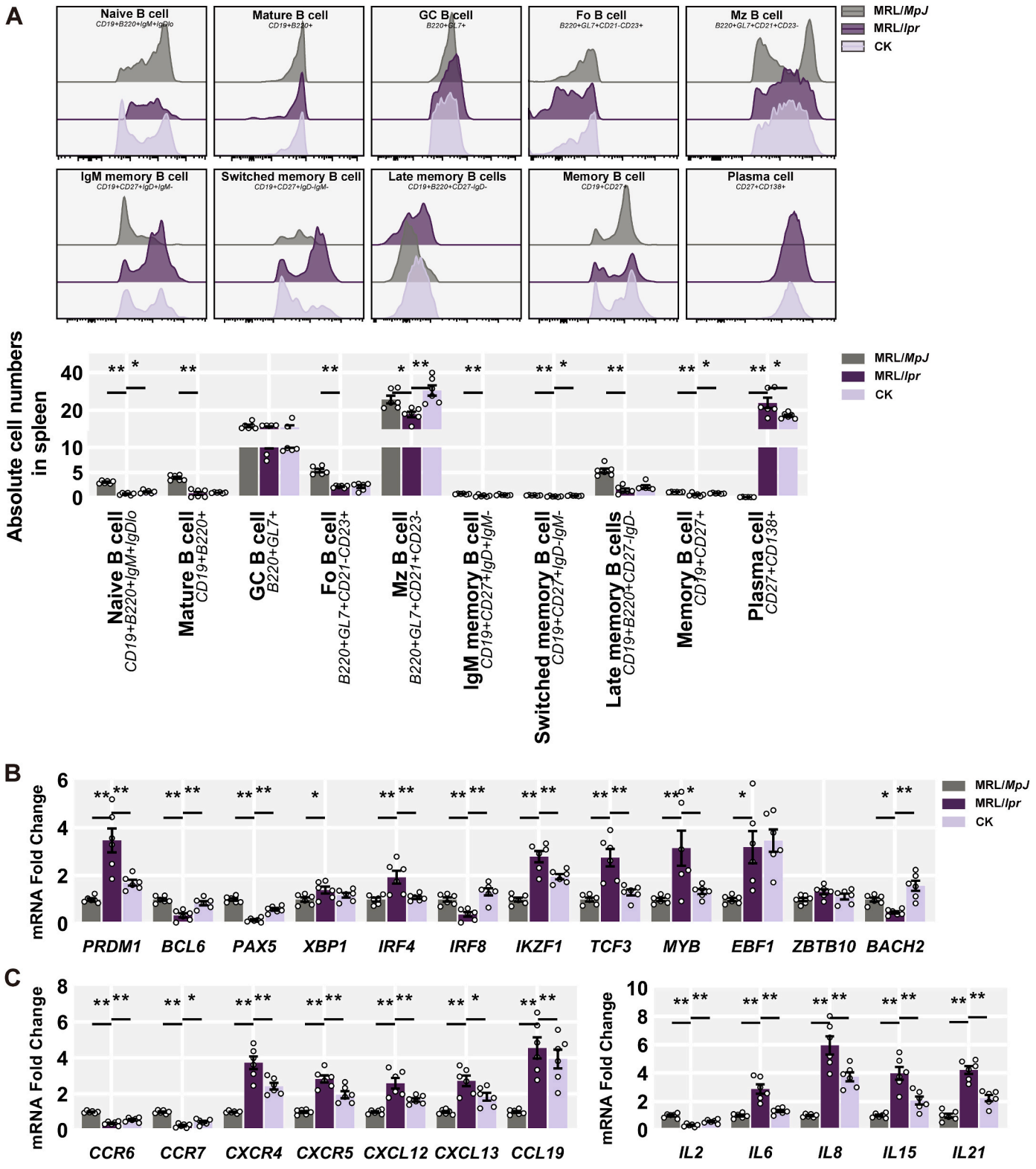


**Fig. 2.** CK re-established splenic B Cell equilibrium. (A) Quantification of splenic B cell subsets. (B) Splenic mRNA levels of B cell activation. (C) Splenic mRNA levels of inflammatory cytokines and chemokines.

(Fig. 3B). Dense deposits of C3 and IgG were abundant in MRL/*lpr* mice glomeruliconversely, there was a significant reduction in the deposition of both in mice treated with CK (Fig. 3C). Moreover, CK inhibited the expression of TGF-β1 and Smad3 in MRL/*lpr* mice glomeruli (Fig. 3D), indicating a reduction in glomerular fibrosis.

Nephrin plays a dominant role in podocyte maturation and slit diaphragm stability [34]. Synaptopodin (SYNPO) facilitates the maintenance and elongation of foot processes in an actin-based configuration [35]. Immunofluorescence analysis revealed decreased nephrin expression in MRL/*lpr* mice, which was elevated in the CK group (Fig. 3E). Western blotting confirmed an increase in both expressions following CK treatment (Fig. 3F). Podocyte structural disorder sprang up all over

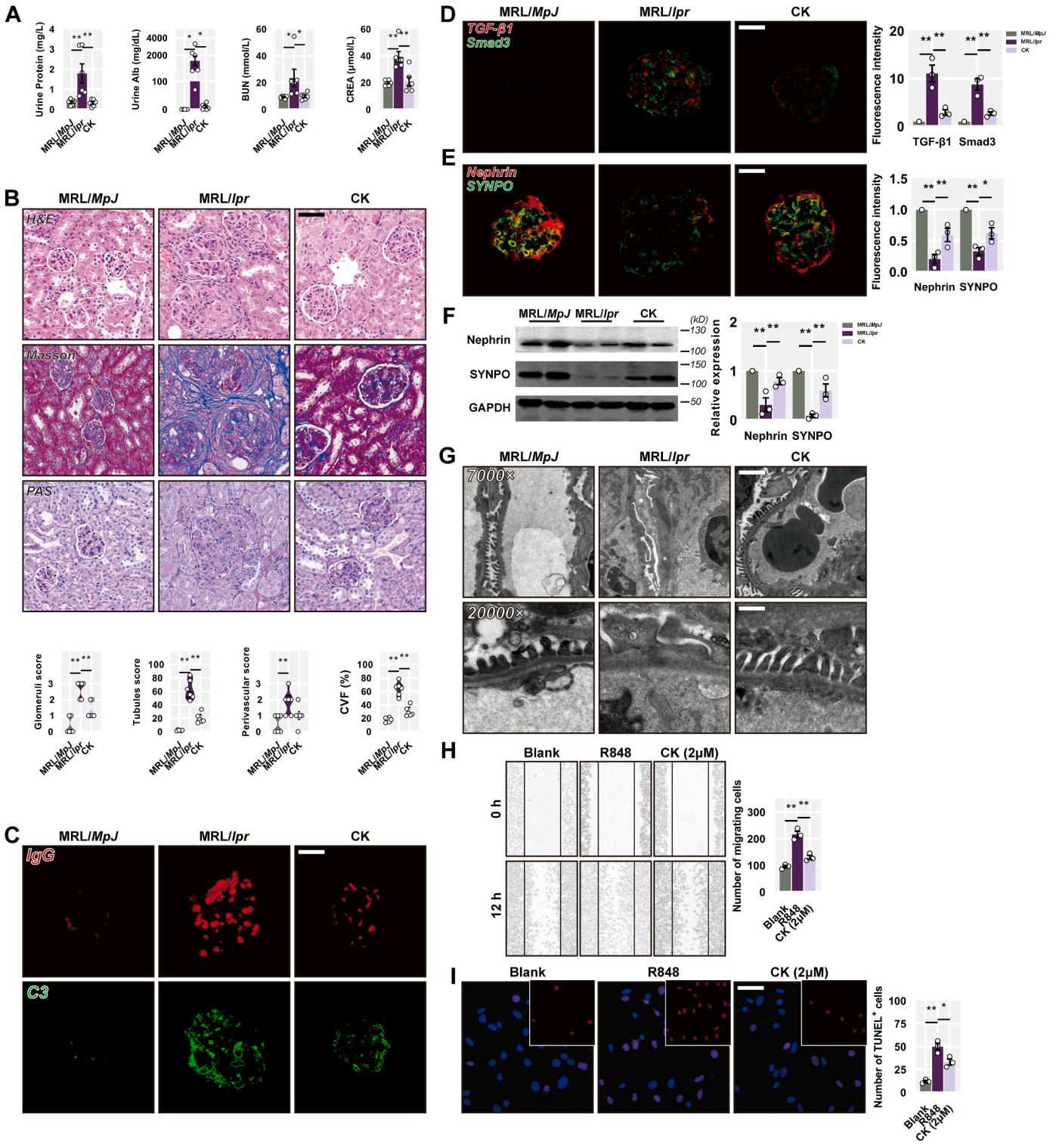


**Fig. 3.** CK restores podocyte ultrastructure following renal damage. (A) Decreased urine protein and albumin levels were found in CK-treated MRL/*lpr* mice, BUN, and creatinine levels among groups, $n = 6$ per group. (B) Representative images of H&E, PAS, and Masson staining. Scale bars: 50 μm. And mean histological scores and collagen volume fraction. (C) C3 and IgG deposition in the glomeruli. (D) Detections of TGF-β1, Smad3, (E) nephrin, and SYNPO staining in the glomeruli, $n = 3$ per group. Scale bars: 20 μm. (F) The expression levels of nephrin, SYNPO, and GAPDH in renal cortex samples. (G) Electron microscopic images from fresh renal cortex samples from the indicated treatment groups. Original magnification, scale bars: 2 μm, × 7000; scale bars: 0.5 μm, × 20,000. (H) Wound healing assay of MPC-5 cells, $n = 3$ per group. (I) Results of TUNEL staining of MPC-5 cells after R848 treatment with or without CK, $n = 3$ per group. Scale bars: 50 μm.

MRL/*lpr* mice displaying the extensive ablation of foot processes and cellular vacuolization, alongside subendothelial granular dense deposits; however, CK treatment partially mitigated these features, embodying the restoration of the ordered arrangement of foot processes (Fig. 3G).

A wound-healing assay was performed on MPC-5 cells to elucidate the effect of CK on podocyte motility under the influence of R848 (a toll-like receptor 7/8 agonist) to replicate the simulated lupus environment [36]. R848-treated podocytes largely repleted the scratch region with

hyperkinetic relative to the normal controls, while CK retarded their motility (Fig. 3H). Additionally, CK effectively prevented R848-induced podocyte apoptosis (Fig. 3I). These findings suggest that CK may counter podocyte detachment and apoptosis, potentially contributing to structural remission.

### 3.4. CK delays the renal conversion into plasma cells

The routine and inevitable occurrence of immune complex deposition is initiated by the colonization of plasma cells in the glomeruli during LN [37]. To meticulously distinguish the role of each B cell subset in patients with LN, we utilized an open-source single-cell RNA sequencing dataset from the renal samples of LN patients [2]. 21 active subsets of leukocytes were annotated, focusing specifically on B cell subpopulations derived from the dataset involving activated B cells, plasma cells and plasmablasts, naive B cells, and ISG-high B cells (Fig. 4A). Local B cell activation and conversion into plasma cells accelerated renal injury (Fig. 4A). We intended to trace various B cell subpopulations in renal samples from MRL/*lpr* mice. Plasma cells notably increased in renal samples of MRL/*lpr* mice, while CK treatment reduced the abundance (Fig. 4B). We took up the aforementioned canonical genes (i.e., B cell activation, inflammation, and chemokines) to identify disparities among B cell subpopulations (Fig. 4C). Consistent with clustered dataset results, increased B cell activation gene expression was observed in renal samples of MRL/*lpr* mice; however, CK treatment suppressed *IRF4* and *MYB* expression (Fig. 4D). Furthermore,

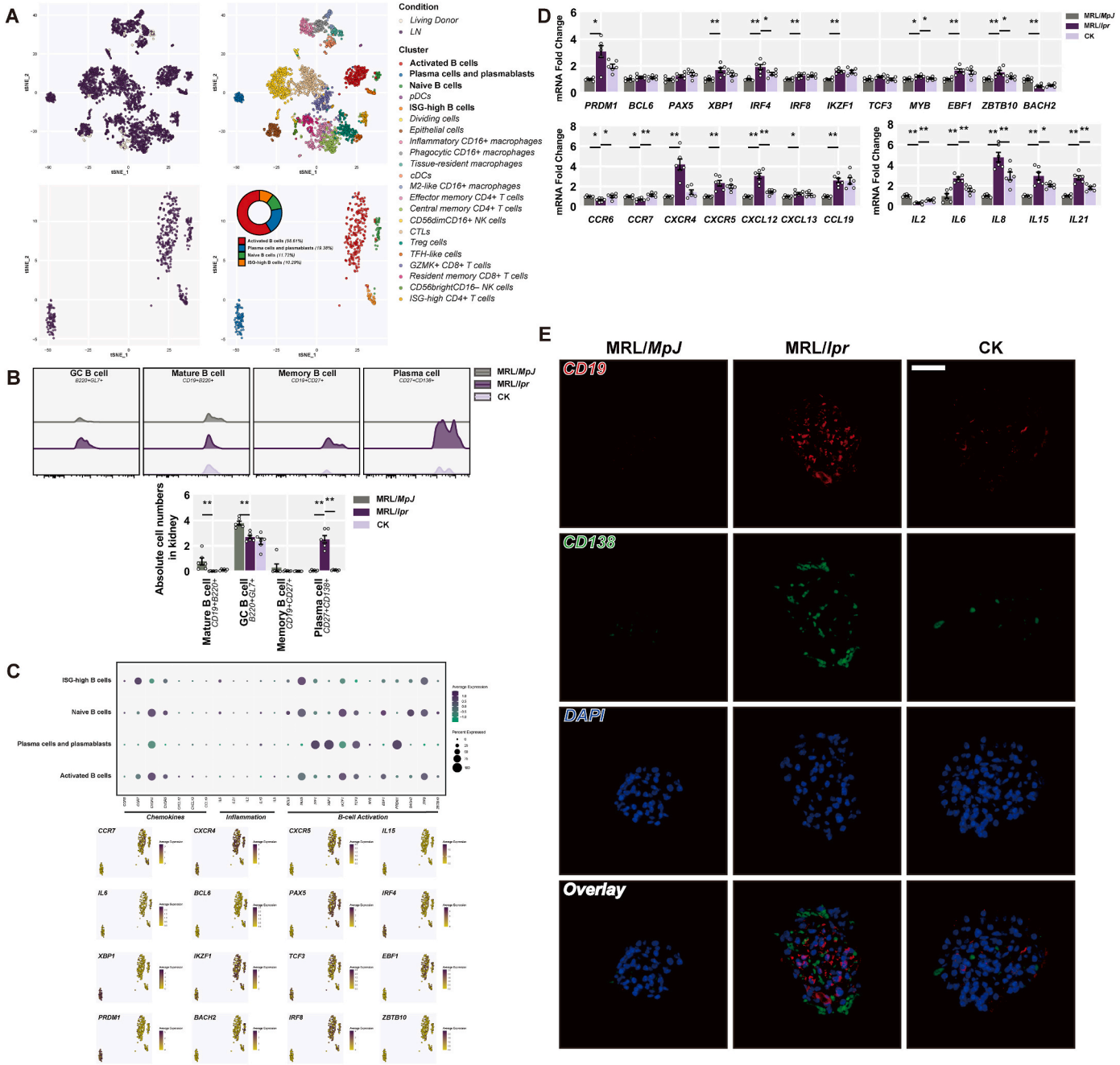


**Fig. 4.** CK delays the renal conversion into plasma cells. (A) Each cell population was annotated and integrated with UMAP. (B) Quantified results of B cells from renal samples. (C) AUCell analysis of mean expression, dot plots, and clustering. (D) Gene expression of B cell activation-associated transcription factors, inflammatory cytokines, and chemokines. (E) The levels of CD19 (red) and CD138 (green) in the glomeruli. Scale bars: 20 μm.

CK inhibited recruitment of B cell subsets to the kidneys in MRL/lpr mice at least partly, along with an overall reduction in inflammation-related genes (Fig. 4D). The number of plasma cells (CD138-positive cells) was higher within the glomeruli of MRL/*lpr* mice compared to control subjects; however, administration of CK induced a notable reduction in this phenomenon (Fig. 4E). The above findings suggest that CK may delay B cell activation and conversion into plasma cells, contributing to renal mitigation.

### 3.5. CK-mediated renal remission depends on rhamnose

To elucidate CK's precise mechanism on renal B cell subsets, non-targeted metabolomics analysis was conducted on renal samples from each group. Metabolite profiles significantly differed among the three groups, suggesting distinct metabolic heterogeneity in response to CK interventions (Fig. 5A). The differential metabolites were screened that could be essentially back-regulated by CK in positive- or negative-ion modes (Fig. 5B and C). Notably, Rhamnose emerged as a key metabolite with the largest effect size (Fig. 5D). Pathway analysis indicated that CK treatment induced various responses in metabolic pathways in MRL/*lpr* mice (Fig. 5E). Additionally, pathway enrichment analysis at the single-cell level identified differences among B cell subpopulations (Fig. 5F). Rhamnose-associated *fructose and mannose metabolism* exhibited significant differences between activated B cells and plasma cells. These findings suggested that CK leans on Rhamnose enrichment to repair LN, and the Rhamnose-relevant pathway might evoke distinct impacts on various B cell subpopulations.

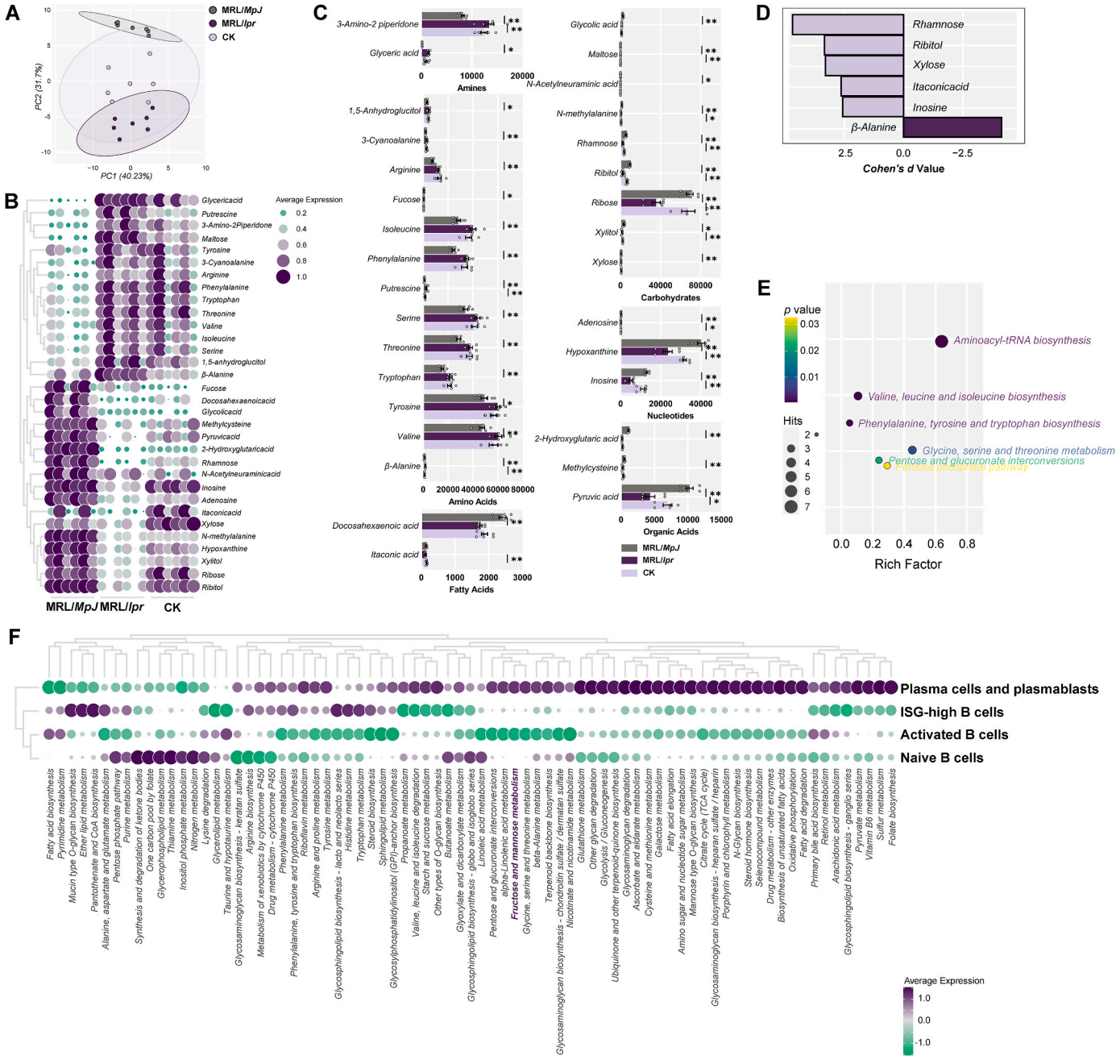


**Fig. 5.** CK-mediated renal remission depends on Rhamnose. (A) PCA plots of metabolites in renal samples. (B) Heatmap and (C) profiles of differential metabolites. (D) Core metabolites were screened by effect size (Cohen's d). (E) Enrichment analysis of renal metabolites for metabolic pathways. (F) SCDE analysis of metabolic pathways in single-cell clusters.

### 3.6. CK induces the B cell-specific activation of SIRT1 and AMPK to resist damage

Rhamnose, a naturally abundant monosaccharide, navigates to catalyze the reversible isomerization of aldose and ketose [38]; it contributes to activating SIRT1 and AMPK [39–41]. We next sought to determine the distinct effects of CK-induced rhamnose enrichment on B cell subsets within the SIRT1/AMPK axis at the single-cell level. Plasma cells and plasmablasts displayed lower *SIRT1* and *PPKAA1* expression than activated B cells during LN, while an opposite trend was observed for the *CPTA1* pattern (Fig. 6A). Molecular docking results indicated favorable binding forces of CK to SIRT1 (−9.5 kcal/mol) and AMPK (−8.1 kcal/mol) (Fig. 6B).

Meanwhile, there was a significant decline in SIRT1 levels, accompanied by reduced AMPK expression in the glomeruli of MRL/*lpr* mice compared to the control group. Conversely, CK treatment resulted in a rebound expression of both SIRT1 and AMPK (Fig. 6C). Immunoblotting analysis of renal samples yielded concordant outcomes for SIRT1 expression (Fig. 6D). Additionally, a lower level of phosphorylated AMPK (*p*AMPK) was observed in MRL/*lpr* mice relative to the control group, while CK treatment seemed to enhance AMPK phosphorylation (Fig. 6D). Furthermore, CK treatment prevented the decrease in CPT1A expression in MRL/*lpr* mice (Fig. 6D).

To explore CK's effects on the SIRT1 network more comprehensively, especially within plasma cells, we utilized Namalwa cells diverged upon in vitro stimulation to induce a plasma cell-like feature. SIRT1 and *p*AMPK expression was reduced in the mimic model group, while CK treatment group. CK treatment markedly upregulated CPT1A expression (Fig. 6E). These findings collectively suggest that CK-induced alleviation of plasma cell accumulation in the glomeruli involves intricate crosstalk mechanisms, specifically through B cell-specific activation of SIRT1 and AMPK.

## 4. Discussion

A detailed description of CK in nephritis benefits proposed previously in NZB/WF1 mice deals with NLRP3 inflammasome in podocytes and macrophages [23]. However, none addresses the B cell subpopulations in LN. Building upon our single-cell level observations, we present a general mechanism through which CK delays the conversion of B cell subgroups into plasma cells, thereby alleviating immune complex deposition primarily through reciprocal regulation between SIRT1 and AMPK. Our study demonstrates that CK treatment is efficacious in mitigating severe proteinuria in MRL/*lpr* mice. Over the intervention period, CK appears to reduce the potential mortality of MRL/*lpr* mice. It accomplishes this through the retention of foot processes, which prevents detachment of podocytes and thereby reestablishes the perm-selective barrier; this process involves sweeping antibodies (anti-dsDNA) with systemic inflammatory attenuation. Mechanically, CK upregulates B cell-specific SIRT expression in agreement with the entire renal one; it serves as a natural agonist of AMPK. This modulation of the SIRT1-AMPK network diminishes the infiltration of chemokine gradient-dependent renal plasma cells, clearing the deposited immune complexes in the glomeruli of MRL/*lpr* mice.

Deposited immune complexes are essential in podocyte injury with an ablated foot process [42]. SYNPO and filamentous actin form the contractile apparatus that anchors podocytes to the underlying substrate [43]. Intravital multiphoton microscopy in three dimensions revealed that podocytes maintain a predominantly quiescent state under normal conditions [44]. However, increased dynamic motility could destabilize this state upon exposure to adriamycin-induced injury [45]. Moreover, the well-formed configuration of foot processes is contingent upon the soundness of the actin cytoskeleton, and the obliteration of podocytes emanates from the vulnerable cytoskeleton due to the loss of filamentous actin [46]. Previous studies have shown CK yields renoprotective effects in a dose-dependent manner, with the most significant improvements observed at a dosage of 40 mg/kg, alongside its anti-inflammatory actions [25]. This aligns with our earlier research highlighting consistent anti-inflammatory potential at the same dosage [19]. Accordingly, investigating the role of CK in LN from a podocyte perspective is valuable beyond the context of inflammation resolution. In the present study, CK demonstrated the potential to restrict motility and promote podocyte attachment. Additionally, our previous works have confirmed that CK could normalize the assembled state of the cytoskeleton [19,47]. Thus, CK might counteract cytoskeleton disruption in podocytes, leading to the preservation of foot process interdigitation. Moreover, recent studies have underscored the critical role of SIRT1 in linking leukocyte-expressed junctional adhesion molecules to lipid accumulation in podocyte injury [14]. Similarly, active AMPK could compensate for the podocyte injury during COX-2 induction [48]. Herein, we demonstrated decreased expression of both SIRT1 and AMPK in MRL/*lpr* mice, while CK treatment activates both proteins, thereby restraining motility and promoting podocyte attachment. Given the similar roles of SIRT1 and AMPK in cellular metabolism and inflammation, theCK-induced increase in Rhamnose content could potentially shift energy balance by reducing long-chain fatty acid levels [39], supported by the upregulation of CPT1A expression observed in our study.

B cells span a continuum of states, from naive to activated, during LN, driving immune responses to local renal damage in situ [49,50]. The renal infiltration and retention of B cells result from the age-associated B cell expansion in a BCR/TLR ligands-dependent action [51]. Moreover, SIRT1-null mice spontaneously develop comprehensive lupus features, including high levels of anti-nuclear antigen immunoglobulins, highlighting the role of SIRT1 in intrinsic B cell mechanisms and epigenetic modulation [52]. This argument aligns that lupus onset attributed to the SIRT1 rs375891 allele, with *rs375891T* postulated as a risk factor for nephritis [15]. Similarly, diminished SIRT1 expression in lupus B cells allows the propulsion of class-switched and somatically hypermutated autoantibodies; it might also contribute to hyperacetylation of Aicda promoter histones in lupus-prone mice and human LN samples [53]. Of note, albeit AMPK appears inconsequential in functional homeostasis of the bone marrow-resident or long-lived plasma cell population, its deletion drives massive immunoglobulin levels in lupus-prone mice; conversely, sustained AMPK activation delays the conversion of other B cell subsets into plasma cells [54]. Initially, CK treatment labors in splenic B cell compensation in MRL/*lpr* mice for the depletion of naive and switched memory B cells and the shrinkage of plasma cell accumulation, and this process might allow the normalization of the spatial distribution of B cell subsets. Specifically, the single-cell level-based genetic mapping on B cell subsets facilitates the discovery: plasmablasts and plasma cells exhibit a lower trend for SIRT1 and AMPK than other subgroups. These findings emphasize the pivotal role of the SIRT1/AMPK axis in dwindling plasma cell expansion during LN, consistent with previous reports [17,53,54]. In line with renal B cell subset results, CK-mediated reduction of renal plasma cell recruitment occurs in response to the lupus microenvironment. More explicitly, this phenomenon leans on the activation of B cell-specific SIRT1 and AMPK to impede the differentiation and proliferation of B cells converting into plasma cells. Meanwhile, our data from renal metabolomics revealed rhamnose as a prominent core metabolite induced by CK, suggesting that CK might counteract stress-induced damage in podocytes leaning on the connection between rhamnose and the SIRT1/AMPK axis. Rhamnose, a versatile activator of SIRT1 and AMPK, has been shown to enhance FoxO1 phosphorylation, boosting SIRT1 expression as well as directly modulating energy metabolism by activating AMPK [40,41]. Thus, CK-mediated modulation of the SIRT1/AMPK network appears to be multifaceted, encompassing both direct regulation and rhamnose enrichment. Nevertheless, there is a current lack of understanding of the immunomodulation of Rhamnose on B cells or lupus. Rhamnose has been shown to inhibit NF-κB and reduce proliferation in colon cancer cell lines [55]; in turn, it could promote macrophage phagocytosis and lymphocyte proliferation, potentially reversing immunosuppression

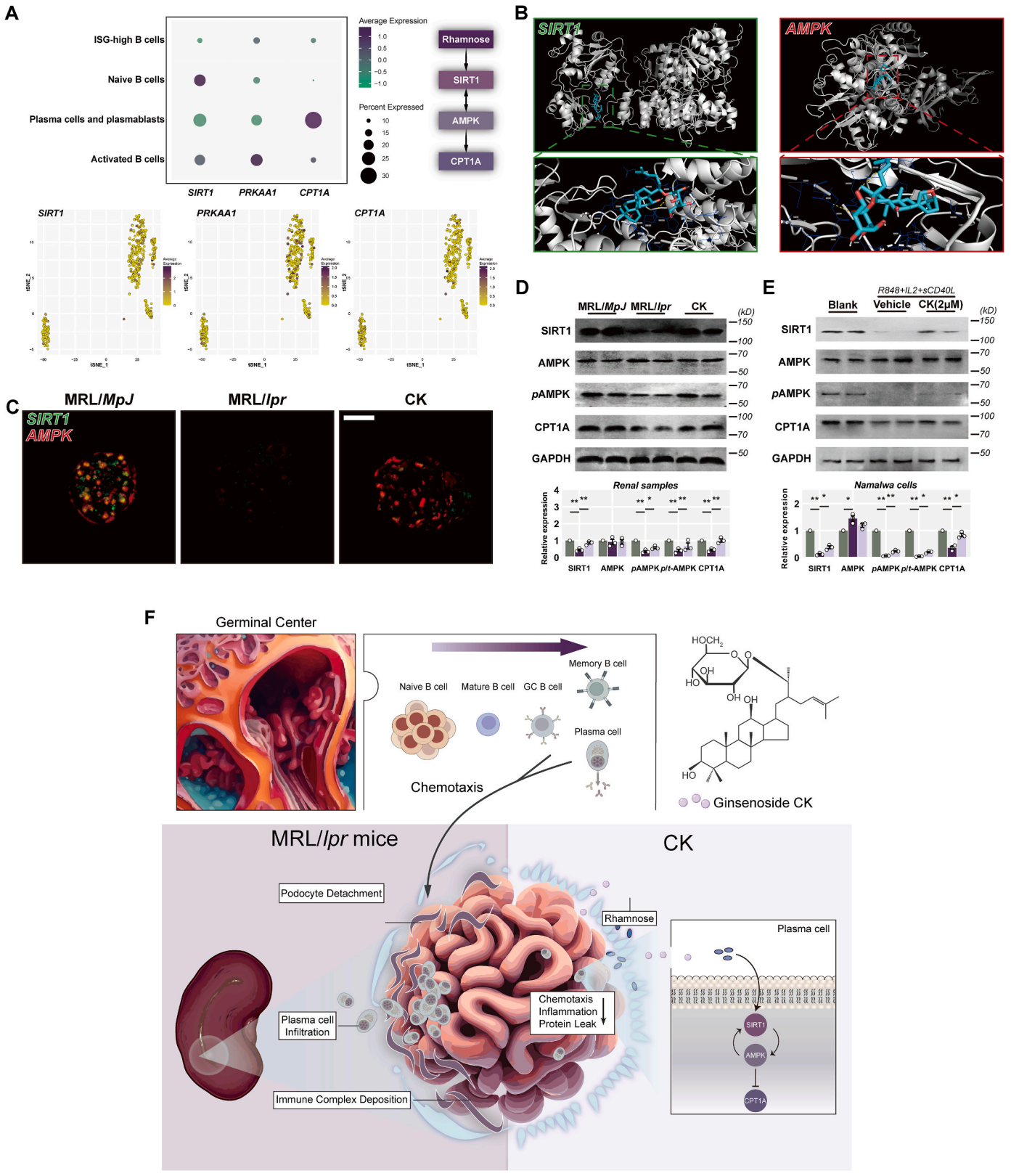


**Fig. 6.** CK induces the B cell-specific activation of SIRT1 and AMPK to resist damage. (A) AUCell analysis of mean expression, dot plots, and clustering. (B) Molecular docking of SIRT1 and AMPK with CK. (C) Detections of SIRT1 and AMPK staining in the glomeruli. Scale bars: 20 μm. (D) and (E) SIRT1, AMPK, *p*AMPK, CPT1A, and GAPDH levels. (F) Diagram illustrating a proposed mechanism for this study.

[56]. Moreover, Rhamnose exhibits anti-fibrotic properties by reducing IL-8 production in dermal fibroblasts [57]. Given these contradictory effects, the elevated Rhamnose levels observed in our study might contribute to mitigating renal inflammation and fibrosis. Nonetheless, a more comprehensive investigation into the functions of Rhamnose is necessary to fully understand its impact on maintaining functional homeostasis during B cell conversion in LN.

Our present study demonstrated that CK might act as a natural agonist of SIRT1 and AMPK in a B cell-specific compensable manner to alleviate nephritis features in lupus-prone mice and potentially reduce mortality. Mechanistically, CK-induced activation of B cell-specific SIRT1 and AMPK, accompanied by Rhamnose accumulation, hindered the conversion of renal B cells into plasma cells. The CK-mediated normalization of nephrin and SYNPO expression, by clearing deposited immune complexes, contributes to the maintenance of podocyte morphology and mobility (Fig. 6F). Our findings underscore the clinical significance of the functional activation of CK in the intricate crosstalk between SIRT1 and AMPK, leading to the amelioration of symptoms in MRL/*lpr* mice and potentially extending to other autoimmune diseases.

## Declaration of competing interest

The authors declare that they have no conflicts of interest.

## Acknowledgments

The authors thank Betty Diamond for sharing the duplicate extraction in the single-cell genomics data. This work was supported by the Project of Zhejiang Provincial Administration of Traditional Chinese Medicine (2020ZZ009, 2021ZX005), the Advantage Discipline Construction Project from Zhejiang Provincial Hospital of Traditional Chinese Medicine (2D02311), the Tangjun Famous Traditional Chinese Medicine Doctor Inherit Workstation Project of Zhejiang Province of China (GZS2021021), and the Huangqi Famous Traditional Chinese Medicine Doctor Inherit Workstation Project of Zhejiang Province of China (GZS2020021).

## Appendix A. Supplementary data

Supplementary data to this article can be found online at https://doi.org/10.1016/j.jgr.2023.11.006.

## References

[1] Martin F, Chan AC. B cell immunobiology in disease: evolving concepts from the clinic. Annu Rev Immunol 2006;24:467–96.
[2] Arazi A, et al. The immune cell landscape in kidneys of patients with lupus nephritis. Nat Immunol 2019;20:902–14.
[3] Furie RA, et al. B-cell depletion with obinutuzumab for the treatment of proliferative lupus nephritis: a randomised, double-blind, placebo-controlled trial. Ann Rheum Dis 2022;81:100–7.
[4] Gregersen JW, Jayne DR. B-cell depletion in the treatment of lupus nephritis. Nat Rev Nephrol 2012;8:505–14.
[5] Murphy G, Isenberg DA. New therapies for systemic lupus erythematosus – past imperfect, future tense. Nat Rev Rheumatol 2019;15:403–12.
[6] Manz RA, Lohning M, Cassese G, Thiel A, Radbruch A. Survival of long-lived plasma cells is independent of antigen. Int Immunol 1998;10:1703–11.
[7] Slifka MK, Antia R, Whitmire JK, Ahmed R. Humoral immunity due to long-lived plasma cells. Immunity 1998;8:363–72.
[8] Radbruch A, et al. Competence and competition: the challenge of becoming a long-lived plasma cell. Nat Rev Immunol 2006;6:741–50.
[9] Haley KE, et al. Podocyte injury elicits loss and recovery of cellular forces. Sci Adv 2018;4:eaap8030.
[10] Wright RD, Beresford MW. Podocytes contribute, and respond, to the inflammatory environment in lupus nephritis. Am J Physiol Ren Physiol 2018;315:F1683–94.
[11] Rodgers JT, et al. Nutrient control of glucose homeostasis through a complex of PGC-1alpha and SIRT1. Nature 2005;434:113–8.
[12] Singh V, Ubaid S. Role of silent information regulator 1 (SIRT1) in regulating oxidative stress and inflammation. Inflammation 2020;43:1589–98.
[13] Su PP, et al. Down-regulation of Risa improves podocyte injury by enhancing autophagy in diabetic nephropathy. Mil Med Res 2022;9:23.
[14] Fu Y, et al. Elevation of JAML promotes diabetic kidney disease by modulating podocyte lipid metabolism. Cell Metabol 2020;32:1052–1062 e8.
[15] Gan H, et al. B cell Sirt1 deacetylates histone and non-histone proteins for epigenetic modulation of AID expression and the antibody response. Sci Adv 2020;6:eaay2793.
[16] Cui J, Bai X, Chen X. Autophagy and diabetic nephropathy. Adv Exp Med Biol 2020;1207:487–94.
[17] Jang SG, et al. Metformin enhances the immunomodulatory potential of adipose-derived mesenchymal stem cells through STAT1 in an animal model of lupus. Rheumatology (Oxford) 2020;59:1426–38.
[18] Kim DH. Gut microbiota-mediated pharmacokinetics of ginseng saponins. J Ginseng Res 2018;42:255–63.
[19] Tian F, et al. Ginsenoside compound K increases glucagon-like peptide-1 release and L-cell abundance in db/db mice through TGR5/YAP signaling. Int Immunopharm 2022;113:109405.
[20] Tian F, et al. Compound K attenuates hyperglycemia by enhancing glucagon-like peptide-1 secretion through activating TGR5 via the remodeling of gut microbiota and bile acid metabolism. J Ginseng Res 2022;46:780–9.
[21] Oh JM, Chun S. Ginsenoside CK inhibits the early stage of adipogenesis via the AMPK, MAPK, and AKT signaling pathways. Antioxidants (Basel) 2022;11.
[22] Kim MS, et al. Compound K modulates fatty acid-induced lipid droplet formation and expression of proteins involved in lipid metabolism in hepatocytes. Liver Int 2013;33:1583–93.
[23] Lin TJ, et al. Accelerated and severe lupus nephritis benefits from M1, an active metabolite of ginsenoside, by regulating NLRP3 inflammasome and T cell functions in mice. Front Immunol 2019;10:1951.
[24] Theofilopoulos AN, Dixon FJ. Murine models of systemic lupus erythematosus. Adv Immunol 1985;37:269–390.
[25] Song W, Wei L, Du Y, Wang Y, Jiang S. Protective effect of ginsenoside metabolite compound K against diabetic nephropathy by inhibiting NLRP3 inflammasome activation and NF-kappaB/p38 signaling pathway in high-fat diet/streptozotocin-induced diabetic mice. Int Immunopharm 2018;63:227–38.
[26] Kosti P, et al. Hypoxia-sensing CAR T cells provide safety and efficacy in treating solid tumors. Cell Rep Med 2021;2:100227.
[27] Yang M, et al. AIM2 deficiency in B cells ameliorates systemic lupus erythematosus by regulating Blimp-1-Bcl-6 axis-mediated B-cell differentiation. Signal Transduct Targeted Ther 2021;6:341.
[28] Schwickert TA, et al. Ikaros prevents autoimmunity by controlling anergy and Toll-like receptor signaling in B cells. Nat Immunol 2019;20:1517–29.
[29] Kikawada E, Lenda DM, Kelley VR. IL-12 deficiency in MRL-Fas(lpr) mice delays nephritis and intrarenal IFN-gamma expression, and diminishes systemic pathology. J Immunol 2003;170:3915–25.
[30] Van Belle K, et al. Comparative in vitro immune stimulation analysis of primary human B cells and B cell lines. J Immunol Res 2016;2016:5281823.
[31] Weinberger M, Simoes FC, Patient R, Sauka-Spengler T, Riley PR. Functional heterogeneity within the developing zebrafish epicardium. Dev Cell 2020;52:574–590 e6.
[32] Liu J, et al. Investigating the mechanisms of jieduquyuziyin prescription improves lupus nephritis and fibrosis via FXR in MRL/lpr mice. Oxid Med Cell Longev 2022;2022:4301033.
[33] Hou LF, et al. Oral administration of artemisinin analog SM934 ameliorates lupus syndromes in MRL/lpr mice by inhibiting Th1 and Th17 cell responses. Arthritis Rheum 2011;63:2445–55.
[34] Li X, et al. Nephrin preserves podocyte viability and glomerular structure and function in adult kidneys. J Am Soc Nephrol 2015;26:2361–77.
[35] Yu H, et al. Synaptopodin limits TRPC6 podocyte surface expression and attenuates proteinuria. J Am Soc Nephrol 2016;27:3308–19.
[36] Yokogawa M, et al. Epicutaneous application of toll-like receptor 7 agonists leads to systemic autoimmunity in wild-type mice: a new model of systemic Lupus erythematosus. Arthritis Rheumatol 2014;66:694–706.
[37] Maeda K, et al. CaMK4 compromises podocyte function in autoimmune and nonautoimmune kidney disease. J Clin Invest 2018;128:3445–59.
[38] Bautista DA, Pegg RB, Shand PJ. Effect of L-glucose and D-tagatose on bacterial growth in media and a cooked cured ham product. J Food Protect 2000;63:71–7.
[39] Choi M, et al. L-rhamnose induces browning in 3T3-L1 white adipocytes and activates HIB1B brown adipocytes. IUBMB Life 2018;70:563–73.
[40] Chu Q, et al. Purified Tetrastigma hemsleyanum vines polysaccharide attenuates EC-induced toxicity in Caco-2 cells and Caenorhabditis elegans via DAF-16/FOXO pathway. Int J Biol Macromol 2020;150:1192–202.
[41] Jiang P, et al. Structure and potential anti-fatigue mechanism of polysaccharides from Bupleurum chinense DC. Carbohydr Polym 2023;306:120608.
[42] Greka A, Mundel P. Balancing calcium signals through TRPC5 and TRPC6 in podocytes. J Am Soc Nephrol 2011;22:1969–80.
[43] Greka A, Mundel P. Cell biology and pathology of podocytes. Annu Rev Physiol 2012;74:299–323.
[44] Brahler S, et al. Intravital and kidney slice imaging of podocyte membrane dynamics. J Am Soc Nephrol 2016;27:3285–90.
[45] Hackl MJ, et al. Tracking the fate of glomerular epithelial cells in vivo using serial multiphoton imaging in new mouse models with fluorescent lineage tags. Nat Med 2013;19:1661–6.
[46] Qu C, et al. Three-dimensional visualization of the podocyte actin network using integrated membrane extraction, electron microscopy, and machine learning. J Am Soc Nephrol 2022;33:155–73.
[47] Tian F, et al. The ginsenoside metabolite compound K stimulates glucagon-like peptide-1 secretion in NCI-H716 cells by regulating the RhoA/ROCKs/YAP signaling pathway and cytoskeleton formation. J Pharmacol Sci 2021;145:88–96.

[48] Agrawal S, Guess AJ, Chanley MA, Smoyer WE. Albumin-induced podocyte injury and protection are associated with regulation of COX-2. Kidney Int 2014;86:1150–60.
[49] Peterson KS, et al. Characterization of heterogeneity in the molecular pathogenesis of lupus nephritis from transcriptional profiles of laser-captured glomeruli. J Clin Invest 2004;113:1722–33.
[50] Davidson A. Editorial: autoimmunity to vimentin and lupus nephritis. Arthritis Rheumatol 2014;66:3251–4.
[51] Myles A, Gearhart PJ, Cancro MP. Signals that drive T-bet expression in B cells. Cell Immunol 2017;321:3–7.
[52] Sequeira J, et al. sirt1-null mice develop an autoimmune-like condition. Exp Cell Res 2008;314:3069–74.
[53] Xu Z, Zan H, Pone EJ, Mai T, Casali P. Immunoglobulin class-switch DNA recombination: induction, targeting and beyond. Nat Rev Immunol 2012;12:517–31.
[54] Zan H, Casali P. Epigenetics of peripheral B-cell differentiation and the antibody response. Front Immunol 2015;6:631.
[55] Cheng D, et al. Inhibitory effect on HT-29 colon cancer cells of a water-soluble polysaccharide obtained from highland barley. Int J Biol Macromol 2016;92:88–95.
[56] Liu N, Dong Z, Zhu X, Xu H, Zhao Z. Characterization and protective effect of Polygonatum sibiricum polysaccharide against cyclophosphamide-induced immunosuppression in Balb/c mice. Int J Biol Macromol 2018;107:796–802.
[57] Novotna R, et al. Hesperidin, hesperetin, rutinose, and rhamnose act as skin anti-aging agents. Molecules 2023;28.